Splitting of the Isoscalar $E2$ Giant Resonance and Evidence of Low-Lying $E0$ Strength in ^{40}Ca

S. Kamerdzhiev,[1,2] J. Speth,[1] and G. Tertychny[1,2]

[1]*Institut für Kernphysik (Theorie), Forschungszentrum Jülich GmbH, D-52428 Jülich, Germany*

[2]*Institute of Physics and Power Engineering, 249020 Obninsk, Russia*

(Received 7 July 1994; revised manuscript received 2 March 1995)

The isoscalar $E2$ giant resonance in ^{40}Ca has been calculated within a microscopic approach which takes into account, in addition to the random-phase-approximation configurations, one-particle–one-hole (1p1h)⊗phonon configurations and the continuum. We reproduce the observed shift of a considerable part of the $E2$ strength to lower energies which gives rise to a nearly uniform distribution. If we add the $E0$ strength calculated within the same approach, then we obtain good agreement with a recent electron scattering experiment, which is a further strong indication for low-lying $E0$ strength.

PACS numbers: 24.30.Cz, 21.10.Re, 27.40.+z

The isoscalar $E2$ giant resonance in ^{40}Ca has been investigated in many experiments (see [1–5], and references therein). A fine structure has been found in (p, p') experiments with an energy resolution of 70 eV [3], which is a challenge for the microscopic theory of giant resonances. It has also been observed that the isoscalar $E2$ strength in ^{40}Ca is split into two major peaks with energies of 14 and 18 MeV [1–5]. The strength is divided in approximately equal parts around these values. In an (α, α', c) experiment [1,2] one observed $(50 \pm 10)\%$ of the $E2$ ($\Delta T = 0$) energy weighted sum rule (EWSR) in the 10–16 MeV interval and in a (p, p') experiment [3] 24.9% of the $E2$ EWSR was observed in the 13.2–16.0 MeV interval. In the following we will concentrate our discussion on the splitting of the isoscalar giant quadrupole resonance (GQR).

So far there is no theoretical explanation for these facts. The random phase approximation (RPA) calculations give only one peak at about 18 MeV [6]. The inclusion of additional "pure" two-particle–two-hole 2p2h configurations [7,8] does not explain the data. Inclusion of 1p1h⊗phonon configurations [9] [without treatment of all the ground state correlations (GSC) induced by the 1p1h⊗phonon configurations] does not give a quantitative explanation, as was noticed by van der Woude [1].

Here we show that the observed low-lying $E2$ strength in ^{40}Ca is connected with more global and general properties of nuclei in the ground state, i.e., the correlations of the ground state (GSC). These correlations also have a strong influence on the excited states, and they are caused by a consistent treatment of configurations more complex than those which are accounted for by the RPA. There are two kinds of GSC. The first kind is a generalization of the well known RPA ground state correlations which give rise to a redistribution of the strength but do not generate new transitions. The second class of GSC modifies the ground state in such a way that new transitions appear between the correlated ground state and 1p1h⊗phonon configurations. In this sense our method is qualitatively different from the RPA approach. We shall demonstrate that this effect is important and that its inclusion gives an explanation of the above-mentioned experimental data in ^{40}Ca.

Although we discuss here ^{40}Ca only, the results are much more general. We expect the same effects in all lighter nuclei. This may be the explanation of the experimental broad $E2$-strength distribution in other lighter nuclei.

In the present work, we perform microscopic calculations of the isoscalar $E2$ giant resonance using the Green's function method [10]. In addition to the RPA configurations, this method allows us to consider more complex 1p1h⊗phonon configurations and also the single-particle continuum. Therefore all the mechanisms which are necessary for a quantitative description of giant resonance widths are included. Our approach is a generalization of the standard theory of finite Fermi systems as developed by Migdal. We start with a Woods-Saxon single-particle basis and use the phenomenological effective interaction of the Landau-Migdal type,

$$F = C_0[f + f'\boldsymbol{\tau}_1 \cdot \boldsymbol{\tau}_2 + (g + g'\boldsymbol{\tau}_1 \cdot \boldsymbol{\tau}_2)\boldsymbol{\sigma}_1 \cdot \boldsymbol{\sigma}_2]\delta(\boldsymbol{r}_1 - \boldsymbol{r}_2), \quad (1)$$

with the density-dependent parameters f and f' [e.g., $f = f_{ex} + (f_{in} - f_{ex})\rho_0(r)$]. Our approach is not self-consistent, but it accounts for a larger class of particle-vibration diagrams than other approaches of this kind [9,11,12]. It also consistently takes into account 1p1h⊗phonon GSC.

The approach has been applied successfully to calculations of the isovector $E1$ [10], $M1$ [13], $E2$ [14], and isoscalar $E0$ [15] resonances in magic nuclei. In these calculations it was shown that the main characteristics of these resonances including the widths and the fine structure of the isoscalar $E2$ resonance in ^{208}Pb [14] are reproduced very satisfactorily. New features were found due to the consistent treatment of GSC induced by 1p1h⊗phonon configurations—in particular the appearance of a noticeable $E0$ strength at the low-energy tails of the isoscalar $E0$ resonances in ^{40}Ca and ^{208}Pb. There is no direct and complete experimental confirmation of the latter so far

(see, however, Refs. [15] and [16] where some evidence of the experimental low-lying $E0$ strength in ^{40}Ca was discussed). Here we shall show that a very similar phenomenon, i.e., a strong low-lying isoscalar $E2$ strength, exists in ^{40}Ca also, and the experiments confirm this.

We formulate the theory in coordinate space because the computational difficulties of the problem are reduced considerably in this representation. This is especially true for the second class of GSC, which is induced by 1p1h⊗phonon configurations. Such a formulation also allows one to consider the single-particle continuum in the RPA part of the problem [6].

We have solved our basic equation for the transition density $\rho(r,\omega)$ which determines the characteristic of the excitations spectrum, viz.,

$$\rho(\boldsymbol{r},\omega) = -\int d\boldsymbol{r}'\, A(\boldsymbol{r},\boldsymbol{r}'\omega)V^0(\boldsymbol{r}') - \int d\boldsymbol{r}'\, A(\boldsymbol{r},\boldsymbol{r}',\omega)F(\boldsymbol{r}')\rho(\boldsymbol{r}',\omega), \quad (2)$$

where V^0 is the external field with frequency ω and F is the Landau-Migdal interaction (1). In this form Eq. (2) is quite similar to the RPA equation in coordinate representation. The only difference is contained in the propagator A. The quantity A is our generalized particle-hole propagator which contains both the RPA part and also the 1p1h⊗phonon part. (Some graphs which determine the 1p1h⊗phonon part of A are shown in [14]). All poles of the 1p1h⊗phonon part of the propagator A have the form $(\varepsilon_p - \varepsilon_h + \omega_{\text{phonon}})$. However, the residues of these poles depend strongly on whether or not we take into account the second class of the diagrams. There may be cases when only these diagrams exist; i.e., all the effect is determined by the 1p1h⊗phonon GSC of the second type. Thus, these new GSC lead not only to a redistribution of the strength, but they also produce new transitions.

We correct the single-particle energies for the effects of the phonon coupling which are explicitly considered in our extended RPA theory to avoid the double counting of the phonon mixing. The single-particle continuum was accounted for in the RPA part of the propagator A (see Ref. [6]). In the 1p1h⊗phonon part we have summed over two shells above and below the Fermi level. The more complex configurations have been taken into account via a smearing parameter $\Delta = 500$ keV. For more details about our method, see [10,13–15] and references therein.

The transition density $\rho(\boldsymbol{r},\omega)$ is connected with the strength function which determines the transition probabilities between the ground state and the excited states and is given by

$$S(\omega) = -(1/\pi)\mathrm{Im}\int d\boldsymbol{r}\, V^{0*}(\boldsymbol{r})\rho(\boldsymbol{r},\omega). \quad (3)$$

In our complex 1p1h⊗phonon configurations we have considered only the two low-lying and most collective phonons, i.e., the first 3^- and 5^- phonons which give the largest contribution for the resonances under consideration [10,15]. The characteristics of the phonons have been calculated within the RPA with the same interaction as given in Eq. (1). The small number of phonons allows us to use the known parameters of the theory of finite Fermi systems [17]. Therefore in the calculations of the phonons as well as in solving Eq. (2) we have used the following well-established values of the Migdal parameters:

$$f_{\text{in}} = -0.002, \quad f'_{\text{ex}} = 2.30, \quad f'_{\text{in}} = 0.76,$$
$$g_{\text{in}} = g_{\text{ex}} = 0.05, \quad g'_{\text{in}} = g'_{\text{ex}} = 0.96,$$
$$C_0 = 300\ \text{MeV fm}^3. \quad (4)$$

(For a more detailed discussion of these questions see Refs. [10,13].) The remaining parameter $f_{\text{ex}} = -1.73$ has been fitted to the phonon experimental energies $E(3^-) = 3.73$ MeV and $E(5^-) = 4.49$ MeV.

The main results of the calculations of the EWSR and of the strength function are given by Table I and in Figs. 1 and 2. Here we use the electromagnetic sum rules,

$$\text{EWSR}_{\text{EM}}(E2) = \frac{50\hbar^2}{8\pi m_p} Z\langle r^2\rangle_p = 16412\ e^2\,\text{fm}^4\,\text{MeV},$$
$$\text{EWSR}_{\text{EM}}(E0) = \frac{2\hbar^2}{m_p} Z\langle r^2\rangle_p = 16500\ e^2\,\text{fm}^4\,\text{MeV}, \quad (5)$$

for $E2$ and $E0$ transitions, respectively. The quantity $\langle r^2\rangle_p = 9.94$ fm^2 was calculated using the proton density distribution obtained from our Woods-Saxon single-particle basis. In the calculations of the $B(EL)$ quantities we have summed only over protons because here one only excites the protons (the small recoil effects were taken into account also). The isoscalar and isovector electromagnetic sum rules used in Table I differ by a factor $Z/A = \frac{1}{2}$ from the definitions in Eq. (5).

In Fig. 1 the results of different theoretical approaches of the electromagnetic $E2$ response are shown. The conventional 1p1h RPA shows one single sharp resonance at about 17 MeV, where the main part of the EWSR is concentrated (dotted curve in Fig. 1). If we include in addition 1p1h⊗phonon configurations but leave out the GSC of the

TABLE I. The electromagnetic EWSR depletion for the $E2$ and $E0$ resonances in ^{40}Ca (in % of the EWSR quantities in e^2 fm^4 MeV given in the left column). IS and IV denote isoscalar and isovector, respectively.

$E_{\min} - E_{\max}$ (MeV)	10–16	10–20.5	5–30	5–55
2^+, EM (EWSR = 16412)	17.2	40.1	64.6	107.1
0^+, EM[a] (EWSR = 16500)	12.04	22.6	52.5	106.8
2^+-IS, EM (EWSR = 8206)	28.2	61.4	90.8	107.2
2^+-IV, EM (EWSR = 8206)	5.0	14.1	31.4	102.0

[a]To compare with experiment [6,16] it is necessary to add $B(E2)$ and $(25/16\pi)B(E0)$ (see text).

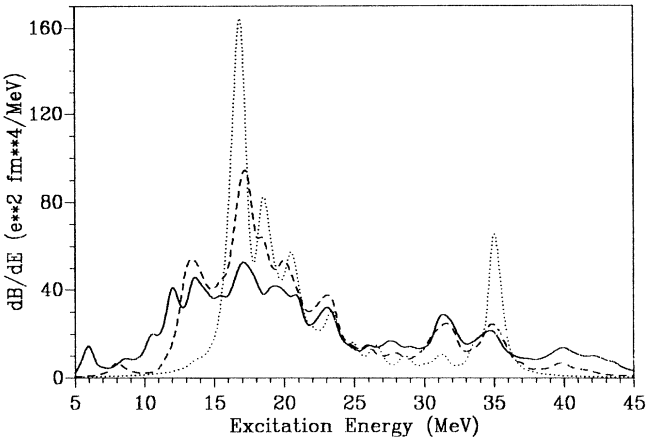

FIG. 1. The calculated $E2$ electromagnetic strength function for ^{40}Ca in the large energy interval. The final results are shown by the solid curve. The RPA+1p1h⊗phonon (without the GSC of the second class) and the continuum RPA results are shown by the dashed and dotted curves, respectively. We expect that the structures seen beyond 25 MeV will be smeared out if more complex configurations are also considered.

second type (dashed curve in Fig. 1), we obtain a splitting of the strength into two major peaks. However, the strength distribution is not in agreement with experiment; we have too little strength below 14 MeV. In our complete calculations we also considered the above-mentioned GSC of the second type which have an important influence on the strength distribution in the low-energy regime. The results are given in the first line of Table I and are shown by the full curve in Fig. 1. We see that the second type of the 1p1h⊗phonon GSC redistributes the EWSR strength in such a way that the strength below 14 MeV increases and the higher part decreases.

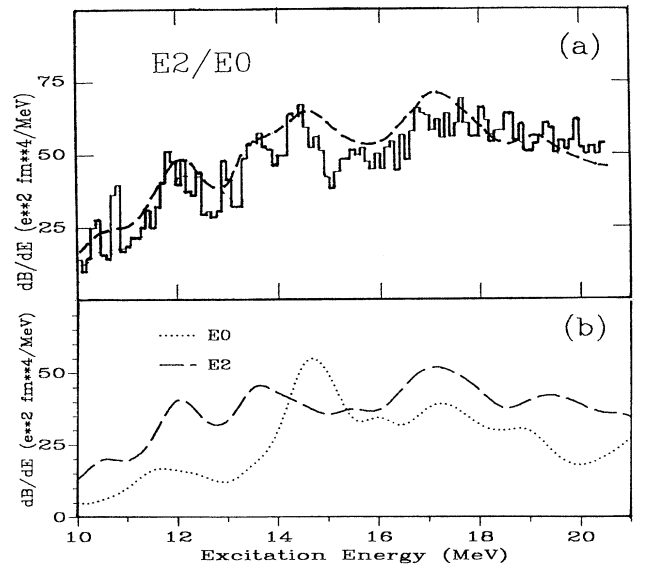

FIG. 2. (a) The experimental data [6] for the strength function vs the theoretical strength function $[dB(E2)/d\omega + (25/16\pi)dB(E0)/d\omega]$. (b) The theoretical electromagnetic $E2$ (dashed line) and $E0$ (dotted line) strength functions. The units are e^2 fm^4 MeV.

In order to compare with electron scattering experiments [5] where the $E2$ and $E0$ multipoles are not disentangled it is necessary to sum the $E2$ and $E0$ strengths in the same proportion as they enter in the longitudinal form factor [18]. Thus we have calculated the quantity $[dB(E2)/d\omega + (25/16\pi)dB(E0)/d\omega]$ and compared it with the experimental data [5] [Fig. 2(a)]. Two main broad maxima at about 14 and 17 MeV and also a third maximum around 12 MeV have been obtained. All the peaks tend to have nearly the same magnitude. Our summed value of the $E2$ plus $E0$ EWSR in the observed interval 10–20.5 MeV is $[6581 + (25/16\pi) \times 3729] = 8436\ e^2$ fm^4 MeV (22% of this quantity is due to the $E0$ contribution). Experiment [16] shows (80 ± 16)% of an EWSR value of 9874 e^2 fm^4 MeV [19], which gives (7899 ± 1580) e^2 fm^4 MeV. Thus we have obtained good agreement with the experimental data.

As shown in Table I we have obtained a full depletion of EWSRs in the 5–55 MeV interval. Inclusion of the second class 1p1h⊗phonon GSC gives an increase of EWSRs by ~7% as compared with the case without these GSC (see Table I, lines 1 and 2).

In the third and fourth lines of Table I we show the results of our calculations of the $E2$ isoscalar and isovector strengths. We see that there is a noticeable contribution of the isovector strength in the 10–20.5 MeV interval and of the isoscalar strength in the 30–55 MeV interval; see also Fig. 1.

Compared to a previous calculation [20] we have changed the $d_{5/2}^{-1}$ and $p_{3/2}^{-1}$ hole energies by adding 2 MeV, which is in agreement with the experimentally known $d_{3/2}^{-1}$-$d_{5/2}^{-1}$ energy difference in ^{39}K [21]. This change does not affect the $E2$-strength distribution below 15 MeV and has only a small effect on the $E0$ distribution. However, it gives an overall energy shift of the higher $B(E2)$ strength by 2 MeV towards lower energies and results in the good agreement with the experimental data [5].

In conclusion, we have found a strong influence of the specific GSC corresponding to the so-called "backward-going" diagrams containing the quasiparticle-phonon interaction for the isoscalar $E2$ and also $E0$ giant resonances in ^{40}Ca. Our calculation of the electromagnetic $E2$ strength gives a nearly uniform distribution in the interval between 12 and 22 MeV. If we consider the isoscalar part only, the $E2$ strength shows more structure, which, however, is washed out by the isovector contribution. We also obtain a well concentrated $E0$ strength around 14.5 MeV which is in agreement with previous experimental claims [16–19,22].

This work was supported by the German-Russian Scientific Exchange Program. The Russian authors thank the leadership of the Institut für Kernphysik, Forschungszen-

trum Jülich, for its hospitality. Useful discussions with N. Frascaria, S. Krewald, P. von Neumann-Cosel, F. Osterfeld, A. Richter, V. Tselyaev, J. Wambach, and A. van der Woude are gratefully acknowledged.

[1] A. van der Woude, in *Electric and Magnetic Giant Resonances in Nuclei,* edited by J. Speth (World Scientific, Singapore, 1991), p. 100.
[2] F. Zwarts *et al.,* Nucl. Phys. **A439**, 117 (1985).
[3] J. Lisantti *et al.,* Phys. Rev. C **40**, 211 (1989).
[4] N. Frascaria, Nucl. Phys. **A569**, 111c (1994).
[5] H. Diesener *et al.,* Phys. Rev. Lett. **72**, 1994 (1994).
[6] S. Shlomo and G. Bertsch, Nucl. Phys. **A243**, 507 (1975).
[7] T. Hoshino and A. Arima, Phys. Rev. Lett. **37**, 266 (1976).
[8] S. Drozdz *et al.,* Nucl. Phys. **A451**, 11 (1986).
[9] P. F. Bortignon and R. A. Broglia, Nucl. Phys. **A371**, 405 (1981).
[10] S. Kamerdzhiev *et al.,* Nucl. Phys. **A555**, 90 (1993).
[11] J. Wambach, V. K. Mishra, and Chu-Hsia Li, Nucl. Phys. **A380**, 285 (1982).
[12] G. Colo *et al.,* Phys. Lett. **276B**, 279 (1992).
[13] S. Kamerdzhiev *et al.,* Z. Phys. A **346**, 353 (1993).
[14] S. Kamerdzhiev, G. Tertychny, and J. Speth, Nucl. Phys. **A569**, 313c (1994).
[15] S. Kamerdzhiev *et al.,* Nucl. Phys. **A577**, 641 (1994).
[16] P. von Neumann-Cosel, in Proceedings of the IV International Conference on Selected Topics in Nuclear Structure, Dubna, Russia, 1994 (Report No. IKDA 94/11).
[17] A. B. Migdal, *Theory of Finite Fermi-Systems and Applications to Atomic Nuclei* (John Wiley, New York, 1967).
[18] G. O. Bolme *et al.,* Phys. Rev. Lett. **61**, 1081 (1988).
[19] P. von Neumann-Cosel (private communication).
[20] S. Kamerdzhiev, J. Speth, and G. Tertychny, Report No. KFA-IKP(TH)-1994-23.
[21] C. M. Lederer and V. S. Shirley, *Table of Isotopes* (John Wiley, New York, 1978).
[22] S. Brandenburg *et al.,* Phys. Lett. **130B**, 9 (1983).